

Edge States at the Interface between Monolayer and Bilayer Graphene

Zi-Xiang Hu^{1,2} and Wenxin Ding³

¹*Department of Physics, ChongQing University, ChongQing, 440004, China*

²*Department of Electrical Engineering, Princeton University, Princeton, New Jersey 08544, USA*

³*NHMFL and Department of Physics, Florida State University, Tallahassee, Florida 32306, USA*

(Dated: November 29, 2018)

The electronic property of monolayer-bilayer hybrid graphene with a zigzag interface is studied by both the Dirac equation and numerical calculation. There are two types of zigzag interface stacks. The dispersion and local density of states behave quite differently along the interface at the Fermi energy due to the different locations of the edge state. We hope our study can give some insights in the understanding of the transport and STM experiments.

PACS numbers: 73.20.At, 73.21.-b, 81.05.U-

I. INTRODUCTION

In recent years, the experimental accessibility of the single and multi layered graphene samples¹⁻⁵ has attracted considerable theoretical and experimental attention due to its unusual electronic structure described by the Dirac equation, namely electrons in monolayer graphene have linear dispersion thus behave like massless Dirac fermions at the corners of the Brillouin zone (BZ)⁶. In the presence of magnetic field perpendicular to the graphene plane, the system shows anomalous integer quantum hall effect⁷⁻¹⁰ (IQHE) which is different from that of the conventional two-dimensional electron system in semiconductor heterostructures. The Hall conductivity in the IQHE of graphene shows half integer plateaus instead of integer ones in the IQHE of a normal semiconductor due to the different degeneracy at $N = 0$ Landau level.

Edge states in graphene have been the focus of much theoretical study because of the important role they play in transport.¹¹ It is well known that there are two basic types of edges in graphene, namely, the armchair and zigzag edges. Some theoretical work¹²⁻²⁶ on the electronic structure of finite-sized systems, either as molecules or as one-dimensional systems, has shown that graphene with zigzag edge has localized edge states at the Fermi energy, but those with armchair edges do not have such state. Therefore, the zigzag edge states is essential to the transport properties in graphene since the localized edge state has contribution to the conductivity. However, most of the work were focused on the uniform monolayer and bilayer graphene. On the other hand the hybrid edge structure composed of partial monolayer and partial bilayer graphene, which is quite general in reality, has received not so much attention. Experimentally,²⁸ the anomalous quantum oscillations in magnetoconductance was observed due to the peculiar physics along the interface. Some of the transport properties and the presence of interface Landau levels was explored within an effective-mass approximation.^{32,33}

In this work²⁹, we study the electronic properties of the hybrid interface systematically via both tight binding

model and its effective theory in the continuum limit - the Dirac equation. The edge states in graphene can be studied experimentally by using a local probe such as scanning tunneling microscopy (STM). The STM experiments measure the differential conductance which is proportional to the density of states. Thus we study the local density of states (LDOS) in different hybridized zigzag edge graphene. It is defined as:

$$N(r, eV) = |\Psi_\alpha(r)|^2 \delta(eV - E_\alpha), \quad (1)$$

where $\Psi_\alpha(r)$ is the eigenfunction with energy E_α . The LDOS shows the strength of the local electronic density which is related to the strength of the signal in STM experimental data. Therefore, the LDOS can show us the signals of the different edge state as in our previous work.²⁷ In this paper, our study of the step edge graphene shows that there are two different zigzag step edge, and there always exists zero energy states localized near the zigzag step edge but the distribution of LDOS of these edge states strongly depends on the details of how the edge stacks together. We find the energy dispersion around the Dirac cones also presents different characters for different edge arrangements either within or without a magnetic field.

This paper is arranged as follows: In section II, we set up the model Hamiltonian in different geometries. The zero energy solutions in zero field and in magnetic field are obtained by solving the Dirac equations and numerical diagonalization is implemented in a finite system in section III and IV, and some discussions and conclusions are in the section V.

II. MODEL AND DIFFERENT GEOMETRIES

We consider the bilayer graphene with AB stacking, as shown in Fig. 1; its tight-binding Hamiltonian can be

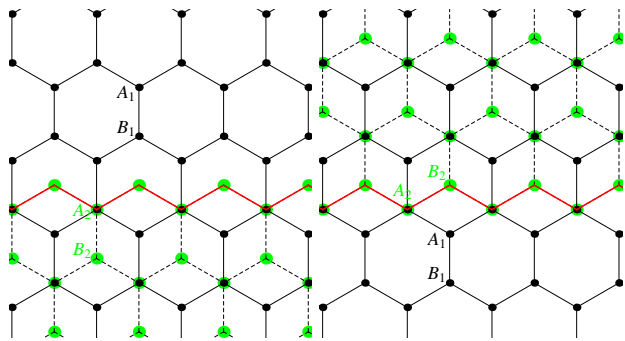


FIG. 1: (Color online) The schematic pictures for two kinds of monolayer-bilayer interface. The atoms of the extended bottom layer (layer 1) are indicated by black dots while the green dots represent the top layer which terminates at the interface. In the left plot, the top layer is ended with B_2 sites (*l.e.b*) while on the right it is ended with A_2 sites (*h.e.b*).

written as:

$$H = -t \sum_{i=1}^2 \sum_{m,n} a_{i;m,n}^\dagger (b_{i;m,n} + b_{i;m-1,n} + b_{i;m,n-1}) - t_\perp \sum_{m,n} a_{2;m,n}^\dagger b_{1;m,n} + h.c., \quad (2)$$

where $a_{i;m,n}$ ($b_{i;m,n}$) is the annihilation operator at position (m, n) in sublattice A_i (B_i), and $i = 1, 2$, indicating the two layers. The first term is the Hamiltonian within each layer, and the second term describes the interlayer coupling in which we only consider the hopping between the two atoms stacked right on top of each other. Let us label the bottom (extended) layer as layer 1, the half plane upper layer as layer 2. In this work we will only consider the $A - B$ (Bernal) stacking. One can expand the effective Hamiltonian near the two Dirac points K and K' which are time reversal symmetric partners. In momentum space, the hamiltonian near K can be written as:

$$H = \sum_k \Psi_k^\dagger \cdot H_k \cdot \Psi_k, \quad (3)$$

where

$$H_k = \begin{pmatrix} 0 & v_F k & 0 & 0 \\ v_F k^* & 0 & t_\perp & 0 \\ 0 & t_\perp & 0 & v_F k \\ 0 & 0 & v_F k^* & 0 \end{pmatrix} = v_F \begin{pmatrix} 0 & k & 0 & 0 \\ k^* & 0 & \gamma & 0 \\ 0 & \gamma & 0 & k \\ 0 & 0 & k^* & 0 \end{pmatrix}, \quad (4)$$

in which $k = k_x + ik_y$, $\gamma = t_\perp/v_F$, and $\Psi_k = (a_{1;k}, b_{1;k}, a_{2;k}, b_{2;k})$. For the other Dirac point, as stated before, $H_{K'} = H_K^*$. Here we only consider the zigzag type interface (or edge) to explore the localized edge state. Without magnetic field and the interface, it is sufficient to discuss just one Dirac cone in the continuum model due to the symmetry. But with the interface breaking the inversion symmetry and the magnetic field breaking

the time reversal symmetry, the two Dirac points are not equal to each other, and both must be studied.

According the lattice orientation we adopt which is shown in Fig. 1, the zigzag interface is along the x direction. For simplicity, we consider an infinite stripe along the x direction, therefore the system has translational symmetry along the x direction thus k_x remains a good quantum number. We then do Fourier transformation in the x direction and reduces the 2D problem to 1D. There are actually TWO distinct geometries which are physically different. i) The outmost sites of the upper layer are the B_2 sites which do not stack directly on the lower layer atoms as showed in Fig. 1(left). The B_2 sites are the low energy degrees of freedom (along with A_1) which are kept if one further considers an 2×2 effective theory on energy scale $\epsilon \ll t_\perp$. We label it the low energy sites boundary (*l.e.b*); ii) the A_2 sites are the outmost sites on the upper layer as showed in Fig. 1(right). The A_2 sites, together with the B_1 sites which they stack right on top of, form the dimer sites. In the 2×2 low energy effective theory the wavefunction have almost zero weight on those dimer sites when $\epsilon \ll t_\perp$. As a result these dimers are ignored in this limit. In other words, they are occupied considerably only at high energy (comparing to t_\perp). Therefore, we shall address such interface as the high energy sites boundary (*h.e.b*).

III. INTERFACE PROPERTIES IN ZERO FIELD

For a semi-infinite sheet, it is well known that the existence of the zero energy edge modes in both monolayer and bilayer graphene. Presumably, such modes are also expected at the interface between them. Let us consider the following geometry: a half plane of monolayer graphene and a half plane of bilayer graphene joined along the zigzag edge; and look for solution(s) with zero eigenenergy by using the Dirac equation.

Before we present the results, let us discuss the boundary conditions at the interface firstly as in Ref. 31. Let

$$\Psi_{\text{mono}}(x, y) = \begin{pmatrix} \psi_A(x, y) \\ \psi_B(x, y) \end{pmatrix} \quad (5)$$

and

$$\Psi_{\text{bi}}(x, y) = \begin{pmatrix} \psi_{A1}(x, y) \\ \psi_{B1}(x, y) \\ \psi_{A2}(x, y) \\ \psi_{B2}(x, y) \end{pmatrix} \quad (6)$$

be the wavefunctions at Dirac point in the monolayer and bilayer respectively. Suppose the interface locate at $y = 0$, the boundary condition for monolayer is then straightforward: both components of the wavefunction must be continuous. For the upper layer, it terminates at $y = 0$ and therefore satisfies the open boundary condition. Note that the term ‘terminates’ indicates the last row of lattice sites are the high/low energy sites, however, the boundary condition is not the wavefunctions

being zero on these sites. They should be the wavefunctions on sites one unit cell ‘outside’ the boundary being zero. To sum up, we have:

$$\begin{cases} \psi_A(x, 0) = \psi_{A1}(x, 0), & \psi_B(x, 0) = \psi_{B1}(x, 0), \\ \psi_{A2}(x, 0) = 0 & \text{l.e.b.} \\ \psi_{B2}(x, 0) = 0 & \text{h.e.b.} \end{cases} \quad (7)$$

In the monolayer region with zigzag interface, we do the substitution $k \rightarrow k_x + \partial_y$ in the Dirac hamiltonian $H_{\text{mono}} = v_F \begin{pmatrix} 0 & k \\ k^* & 0 \end{pmatrix}$.¹¹ The zero energy solution is

$$\begin{cases} \phi_A(y) = e^{yk_x} C_2 \\ \phi_B(y) = e^{-yk_x} C_1 \end{cases} \quad (8)$$

In analogy, we do the same substitution in the bilayer Hamiltonian (Eq. 4) and obtain its zero energy solution:

$$\begin{cases} \phi_{B1}(y) = e^{-yk_x} A_1 \\ \phi_{B2}(y) = -e^{-yk_x} y \gamma A_1 + e^{-yk_x} A_2 \\ \phi_{A1}(y) = e^{yk_x} A_3 + e^{yk_x} y \gamma A_4 \\ \phi_{A2}(y) = e^{yk_x} A_4 \end{cases} \quad (9)$$

Applying the requirement that the wavefunctions remain finite at infinity, for the *l.e.b.* interface (so $\phi_{A2}(y = 0) = 0$), one easily find that nonzero solutions only exist for $k_x > 0$. The solution is

$$C_1 = C_2 = A_1 = A_3 = A_4 = 0, \quad A_2 = \text{const.} \quad (10)$$

For the *h.e.b.* interface, one finds that for $k_x > 0$

$$C_1 = C_2 = A_1 = A_2 = A_3 = 0, \quad A_4 = \text{const.} \quad (11)$$

For the other Dirac cone, the solutions remain the same but only exist for $k_x < 0$. The only nonzero constant is to be determined by normalization. Both results are in agreement with tight-binding analysis³⁰.

Even though the zero energy states exist for both types of interface, there is an important difference between them. In the *l.e.b.* case, the wavefunction is only nonzero in the upper layer, which is trivial as such mode is expected when a graphene sheet is terminated at a zigzag edge. However, the *h.e.b.* is less trivial. The wavefunction also lives on the extended layer at the interface where no cut is present. We interpret this as, when the dimer sites are the boundary, the interlayer coupling t_{\perp} imposes an energy cost for electrons to go through the interface in the extended layer which can be considered as an effective potential barrier. The potential barrier can localize the electron states along the interface.

We numerically diagonalize a system with a finite width up to 600 unit cells in the y direction. The intralayer hopping strength t is set to identity and the interlayer hopping strength $t_{\perp} = 0.2t$. The dispersion relation is shown in Fig. 2. Compare the dispersions in different geometries, the *h.e.b.* edge has an obviously

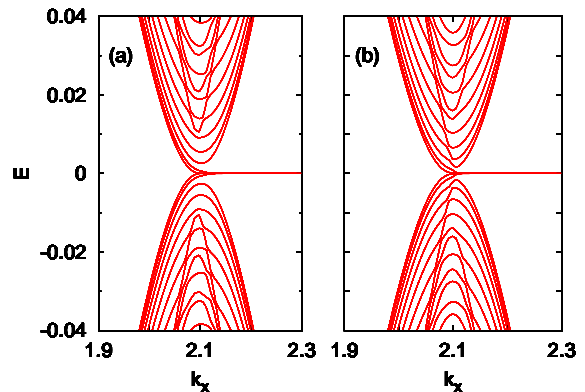


FIG. 2: The dispersion around Dirac cone for the step graphene with (a)*l.e.b.* and (b)*h.e.b.* respectively.

stronger level anti-crossing feature than the other. The reason is that for *l.e.b.* edge, the zero energy edge state just locates on the bilayer graphene which has quadratic dispersion and has nothing to do with the monolayer part with a linear dispersion. However, in the case of *h.e.b.*, the zero energy edge state also has component on the monolayer graphene at the interface, the linear dispersion part for monolayer should also connect to the edge state which induces more energy level anticrossing around the Dirac points. Fig.3 shows the LDOS for the two kinds of step graphene. We label the coordinate of the extended layer by $d \in [0, 600)$ and the $d \in [900, 1200)$ for upper layer. Therefore, the interface locates at $d = 300$ and $d = 900$ for layer 1 and 2 respectively. One can notice that the localized edge state shows as a peak at zero energy along the interface. The prominent difference is that the peak just appears on the top layer of bilayer part in the *l.e.b.* case; but for the *h.e.b.* case, the zero energy peak appears on both two layers although still locates at the bilayer side. The numerical results are in agreement with the analysis by the Dirac equations and we conclude that the two kinds of edge arrangements should have different consequences in experiments since the different distributions of the zero mode. Here we notice that the other peaks in LDOS at the end of the finite system is the signal of the general monolayer or bilayer zigzag edge graphene as discussed in many others work.^{12–26}

IV. INTERFACE PROPERTIES IN MAGNETIC FIELDS

In the presence of magnetic field, by minimal coupling the Dirac equation should be modified by doing the substitution $\mathbf{k} \rightarrow \mathbf{k} + \frac{e\mathbf{A}}{c}$. Assume the magnetic field is along the direction of perpendicular to the plane $\vec{B} = B\hat{z}$, $B > 0$. We adopt the Landau gauge here $\vec{A} = (A_x, A_y) = (-yB, 0)$ due to the translational invariant along x direction. Thus the Hamiltonian of mono-

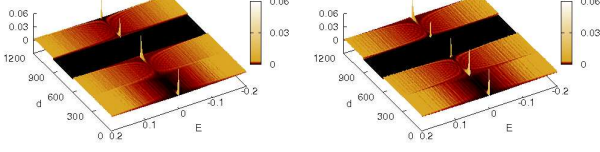


FIG. 3: (color online) The LDOS of the step bilayer graphene with l.e.b.(left) and h.e.b.(right) respectively. The width of monolayer $L = 600$. In plot, the region $d \in [0 : 600)$ stands for the lower extended layer and $d \in [600, 1200)$ is the upper layer.

layer becomes:

$$H_{\text{mono}} = \begin{pmatrix} 0 & k_x + \partial_y - \frac{eBy}{c} \\ k_x - \partial_y - \frac{eBy}{c} & 0 \end{pmatrix}. \quad (12)$$

and its zero energy solution is

$$\begin{cases} \phi_A(y) = C_1 e^{k_x y - \frac{eB}{2c} y^2} \\ \phi_B(y) = C_2 e^{-k_x y + \frac{eB}{2c} y^2} \end{cases} \quad (13)$$

Similarly, the zero energy solution for bilayer graphene becomes:

$$\begin{cases} \phi_{A1}(y) = (A_3 \gamma y + A_2) e^{k_x y - \frac{eB}{2c} y^2} \\ \phi_{B1}(y) = A_1 e^{-k_x y + \frac{eB}{2c} y^2} \\ \phi_{A2}(y) = A_3 e^{k_x y - \frac{eB}{2c} y^2} \\ \phi_{B2}(y) = (-A_1 \gamma y + A_4) e^{-k_x y + \frac{eB}{2c} y^2} \end{cases}. \quad (14)$$

Apply the same boundary conditions as in the zero field case, we will have the solutions. For *l.e.b.*, one gets

$$C_2 = A_1 = A_3 = A_4 = 0, \quad C_1 = A_2 = \text{const}. \quad (15)$$

For *h.e.b.* the solution is

$$C_2 = A_1 = A_4 = 0, C_1 = A_2 = \text{const}_1, A_3 = \text{const}_2. \quad (16)$$

The constants are to be determined by normalization conditions. One immediately notices that the wavefunction lives only on the A sublattice. We should note that on the other Dirac point, the solutions remain the same form, but resides on the B sublattice. Another important feature of the solution is that for *h.e.b.* we actually have TWO independent solutions here.

A. Dispersion Relation

The general problem in magnetic field can be written as

$$\frac{1}{\sqrt{2}} \begin{pmatrix} 0 & \partial_\xi + \xi \\ -\partial_\xi + \xi & 0 \end{pmatrix} \Psi_{\text{mono}} = \epsilon \Psi_{\text{mono}}, \quad (17)$$

for the monolayer while that for the bilayer is

$$\frac{1}{\sqrt{2}} \begin{pmatrix} 0 & \partial_\xi + \xi & 0 & 0 \\ -\partial_\xi + \xi & 0 & \tilde{\gamma} & 0 \\ 0 & \tilde{\gamma} & 0 & \partial_\xi + \xi \\ 0 & 0 & -\partial_\xi + \xi & 0 \end{pmatrix} \Psi_{\text{bi}} = \epsilon \Psi_{\text{bi}} \quad (18)$$

where $\xi = \frac{y}{l_B} - l_B k_x$, $l_B = \sqrt{\frac{c}{eB}}$, $\epsilon = \frac{E}{\omega_c}$, $\omega_c = \sqrt{2} \frac{v_F}{l_B}$, $\tilde{\gamma} = \frac{\gamma}{v_F \omega_c}$. It is known that in the bulk, the solution to the monolayer is

$$\Psi_{\text{mono}} = \begin{pmatrix} \frac{1}{\Gamma(\epsilon^2)} D_{\epsilon^2-1}(\sqrt{2}\xi) \\ \pm \frac{1}{\Gamma(\epsilon^2+1)} D_{\epsilon^2}(\sqrt{2}\xi) \end{pmatrix} = \begin{pmatrix} \psi_{\epsilon^2-1}(\xi) \\ \pm \psi_{\epsilon^2}(\xi) \end{pmatrix}, \quad (19)$$

where the $\epsilon = \pm\sqrt{N}$, $N = 0, 1, 2, \dots$, and D_ν 's are the parabolic cylinder functions, which combined with the factor $1/\Gamma(\nu+1)$ give us the eigen wavefunctions of a harmonic oscillator $\psi_\nu(\xi)$. The bulk solution to the bilayer Hamiltonian can be written in a similar way:

$$\Phi_{\text{bi}} = \begin{pmatrix} \frac{\epsilon(\epsilon^2-(j+1)-\tilde{\gamma}^2)}{\tilde{\gamma}\sqrt{j(j+1)}} \psi_{j-1} \\ \frac{\epsilon^2-(j+1)}{\tilde{\gamma}\sqrt{j+1}} \psi_j \\ \frac{\epsilon}{\sqrt{j+1}} \psi_j \\ \psi_{j+1} \end{pmatrix}, \quad (20)$$

where $\epsilon = \pm\sqrt{1+\tilde{\gamma}^2+2j \pm \sqrt{(1+\tilde{\gamma}^2)^2+4\tilde{\gamma}^2 j}}$ ($j = 0, 1, 2, \dots$) is the eigen energy.

However, for the interface problem, we need solutions on the half-plane. In this case, we let the bilayer live on the $y > 0$ side, so the monolayer is on the $y < 0$ part. Therefore, for the bilayers, the solutions on $(0, \infty)$ take on the same form as in the bulk, but j 's are no longer required to be integers. Instead, we now should replace j 's by

$$j_{1,2} = \epsilon^2 - \frac{1}{2} \pm \sqrt{\epsilon^2 \tilde{\gamma}^2 + \frac{1}{4}}, \quad (21)$$

and ϵ now varies continuously. For the monolayer, the solution on $(-\infty, 0)$ can be chosen as

$$\Psi_{\text{mono}} = \begin{pmatrix} \psi_{\epsilon^2-1}(-\xi) \\ \mp \psi_{\epsilon^2}(-\xi) \end{pmatrix}. \quad (22)$$

With the above solutions, and combined with the boundary conditions that are already discussed in the zero field cases, we obtain the transcendental equations that dictates the dispersion relations. For the *l.e.b.* interface,

$$\begin{aligned} & (\epsilon^2 - (j_1 + 1)) D_{j_1-1}(-\sqrt{2}k_x) (D_{\epsilon^2}(\sqrt{2}k_x) D_{j_2}(-\sqrt{2}k_x) \\ & + D_{\epsilon^2-1}(\sqrt{2}k_x) D_{j_2+1}(-\sqrt{2}k_x)) \\ & = (\epsilon^2 - (j_2 + 1)) D_{j_2-1}(-\sqrt{2}k_x) (D_{\epsilon^2}(\sqrt{2}k_x) D_{j_1}(-\sqrt{2}k_x) \\ & + D_{\epsilon^2-1}(\sqrt{2}k_x) D_{j_1+1}(-\sqrt{2}k_x)), \end{aligned} \quad (23)$$

where we have set $l_B = 1$. For the *h.e.b.*, the dispersion equation is

$$\begin{aligned} & (\epsilon^2 - (j_1 + 1) - \gamma^2) D_{j_1}(-\sqrt{2}k_x) (D_{\epsilon^2}(\sqrt{2}k_x) D_{j_2}(-\sqrt{2}k_x) \\ & \quad + D_{\epsilon^2-1}(\sqrt{2}k_x) D_{j_2+1}(-\sqrt{2}k_x)) \\ = & (\epsilon^2 - (j_2 + 1) - \gamma^2) D_{j_2}(-\sqrt{2}k_x) (D_{\epsilon^2}(\sqrt{2}k_x) D_{j_1}(-\sqrt{2}k_x) \\ & \quad + D_{\epsilon^2-1}(\sqrt{2}k_x) D_{j_1+1}(-\sqrt{2}k_x)) \end{aligned} \quad (24)$$

However, one must note that in the presence of magnetic field, the time reversal symmetry is broken, therefore, the other Dirac cone, the time reversal partner, no longer behaves the same way. So the dispersion relation must be calculated separately. By the same approach, one can get, for the *l.e.b.*,

$$\begin{aligned} & (\epsilon^2 - j_1) D_{j_1}(-\sqrt{2}k_x) (j_2 D_{\epsilon^2}(\sqrt{2}k_x) D_{j_2-1}(-\sqrt{2}k_x) \\ & \quad + \epsilon^2 D_{\epsilon^2-1}(\sqrt{2}k_x) D_{j_2}(-\sqrt{2}k_x)) \\ = & (\epsilon^2 - j_2) D_{j_2}(-\sqrt{2}k_x) (j_1 D_{\epsilon^2}(\sqrt{2}k_x) D_{j_1-1}(-\sqrt{2}k_x) \\ & \quad + \epsilon^2 D_{\epsilon^2-1}(\sqrt{2}k_x) D_{j_1}(-\sqrt{2}k_x)); \end{aligned} \quad (25)$$

for the *h.e.b.*,

$$\begin{aligned} & (j_2 + 1) (\epsilon^2 - j_1 - \gamma^2) D_{j_1}(-\sqrt{2}k_x) (j_2 D_{\epsilon^2}(\sqrt{2}k_x) \\ & \quad D_{j_2-1}(-\sqrt{2}k_x) + \epsilon^2 D_{\epsilon^2-1}(\sqrt{2}k_x) D_{j_2}(-\sqrt{2}k_x)) \\ = & (j_1 + 1) (\epsilon^2 - j_2 - \gamma^2) D_{j_2}(-\sqrt{2}k_x) (j_1 D_{\epsilon^2}(\sqrt{2}k_x) \\ & \quad D_{j_1-1}(-\sqrt{2}k_x) + \epsilon^2 D_{\epsilon^2-1}(\sqrt{2}k_x) D_{j_1}(-\sqrt{2}k_x)). \end{aligned} \quad (26)$$

It is easy to see from the dispersion equation that when $|k_x|$ is very large, the eigen-energy should restore to either the monolayer value or the bilayer value as the parabolic cylinder functions D_ν only converge to zero for integer ν at infinity. But what interests us is how these bulk Landau levels connect with each other when crossing the interface. To study that, we solve the above equations for ϵ and k_x near the interface $k_x = 0$ for a finite size system as shown in Fig. 4. We see that at the two Dirac cones, the Landau levels match in different ways. Furthermore, we present the numerical result for directly diagonalizing a ribbon with width $L = 600$. Our diagonalization results consistent with the analytic analysis also. Fig. 5 and Fig. 6 shows the energy spectrum and LDOS for step bilayer graphene in a magnetic field with *l.e.b.* and *h.e.b.* respectively. In magnetic field the energy spectrum is split into a set of Landau levels (LLs) and the Landau level splitting in bilayer is smaller than that of monolayer graphene since the energy of LLs in bilayer system satisfies $E \propto \sqrt{n(n-1)}$ and $E \propto \sqrt{n}$ in monolayer. Therefore, LLs are not matched at the interface.

The major difference between the two sets of dispersion relation is that the Landau levels in the two distinct regions connect in two different ways. The dispersion at the interface with *l.e.b.* is more flat than that with *h.e.b.*. These interface Landau levels were discussed by

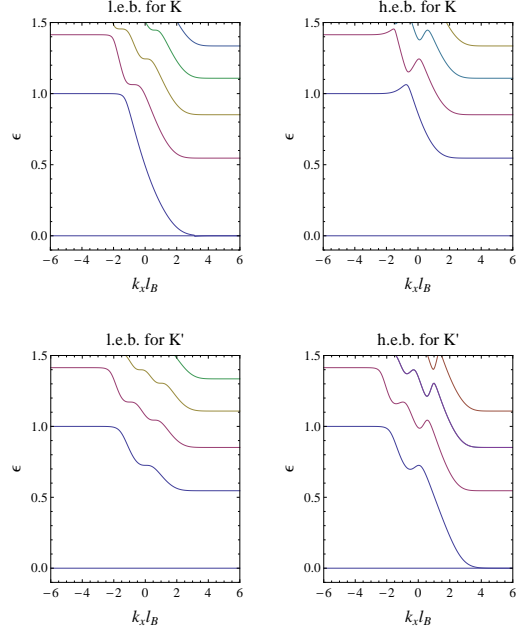


FIG. 4: (color online) The dispersion around Dirac cones in the presence of magnetic field. The upper two figures are for the *l.e.b.* and *h.e.b.* interfaces around one Dirac cone respectively, and the lower two figures are that for the other Dirac cone.

M. Koshino et al. within an effective-mass approximation³². From the plot of LDOS, the same as in the case of zero field, according to the different distribution of the edge state, the presence of the peak at $E = 0$ along the interface only on the upper layer for *l.e.b.* and on both two layers for *h.e.b.*.

We also use the Dirac equation result to study how the dispersive Landau levels near the interface changes when the magnetic field varies. If we measure the energy in unit of $\hbar\omega_c$, the monolayer bulk Landau levels remain unchanged as the magnetic field is being tuned; but for the bilayer, the effective interlayer coupling $\tilde{\gamma} \sim 1/\omega_c$ so the bulk Landau levels vary with the magnetic field. In strong field $\tilde{\gamma} \sim 0$, so the two layers behave as if they were decoupled, and the Landau levels' energy becomes just like the monolayer's but with a two-fold degeneracy. In weak field limit, $\tilde{\gamma} \sim \infty$, in this case one gets $\epsilon \simeq \sqrt{n(n-1)}/\tilde{\gamma}$. The dispersions for $\tilde{\gamma} \in 0.2, 1, 2, 5$ of both *l.e.b.* and *h.e.b.* at one Dirac point are shown in Fig. 7 and Fig. 8 respectively. Here we only plot the Landau levels up to $n = 6$. The evolution of dispersion on the other Dirac point have the similar behavior except different energy level connection as shown in Fig. 4. As the strength of the magnetic field is increased, the bilayer LLs become more denser which induces more mediate states around the interface. The dispersion of the *l.e.b.* interface is always more flat than that of *h.e.b.* interface while tuning the magnetic field.

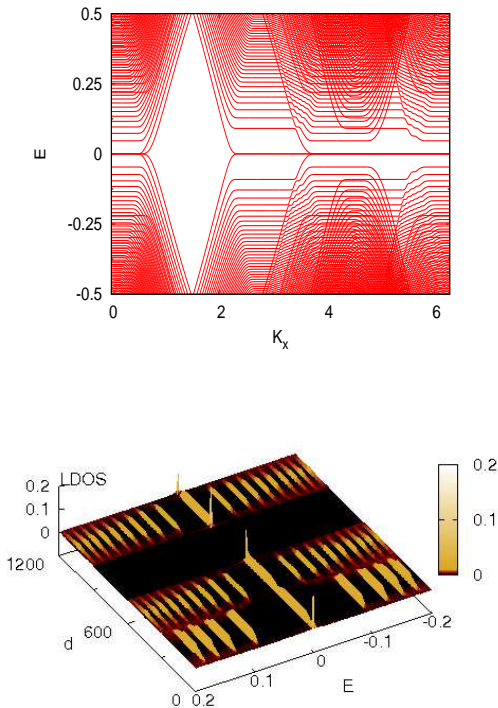


FIG. 5: The energy spectrum and LDOS of the step bilayer graphene with *l.e.b.* in a magnetic field. The strength of the magnetic field is expressed as magnetic flux ϕ in each unit cell. Here we set the magnetic flux per each unit cell $\phi = \phi_0/1315$ (ϕ_0 is the magnetic flux quanta) which corresponds to $B \sim 60T$.

V. DISCUSSION AND CONCLUSION

In this paper, we discuss the edge state at the interface between monolayer and bilayer graphene. Physically, there are two types of interface structures named by the *l.e.b.* and *h.e.b.* due to the different terminations at the interface. By studying the system with both effective theory and numerical calculation, we find that with or without magnetic field, zero energy edge states exist for both types of interface, however, the LDOS shows different features. For *l.e.b.* the zero energy edge states only live in the upper layer which terminates at the interface while the *h.e.b.* induces an enhanced LDOS in the bottom layer. Another major difference between the two different geometries is that the dispersion of *h.e.b.* system shows a stronger anticrossing feature in the zero field. Both differences can be interpreted as the following. When an electron goes through the *h.e.b.* interface, it can choose to lower its energy through the interlayer coupling. This can be viewed as the *h.e.b.* imposes an effective potential barrier at interface in the extended layer. Since the localized zero energy edge states locates on both two layers, the monolayer dispersion which is linear should smoothly connect to the edge state in the *h.e.b.* case. This can explain the strong energy level an-

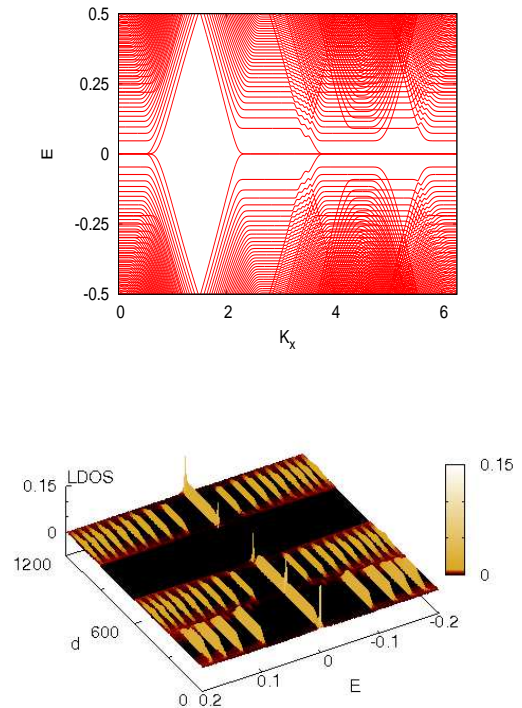


FIG. 6: The energy spectrum and LDOS of the step bilayer graphene with *h.e.b.* within magnetic field. The parameters are the same as in Fig. 5

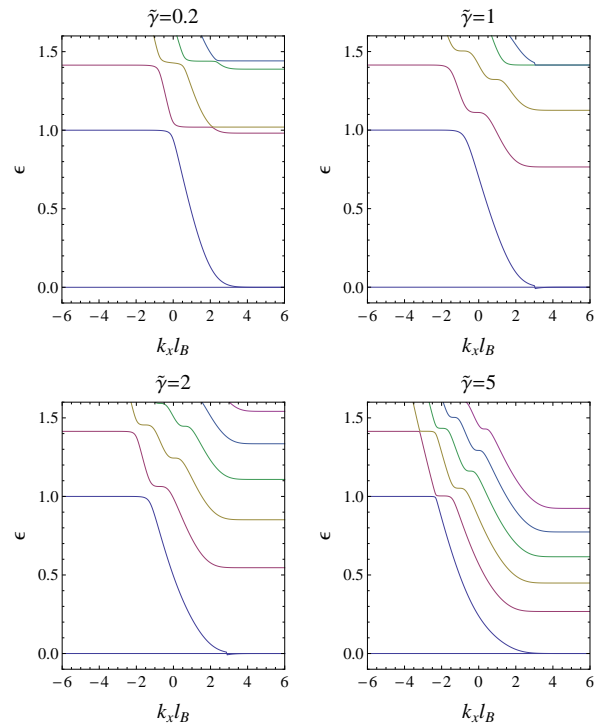


FIG. 7: The dispersion around Dirac cones K of *l.e.b.* type interface in different magnetic field with $\tilde{\gamma} = 0.2, 1, 2, 5$ respectively.

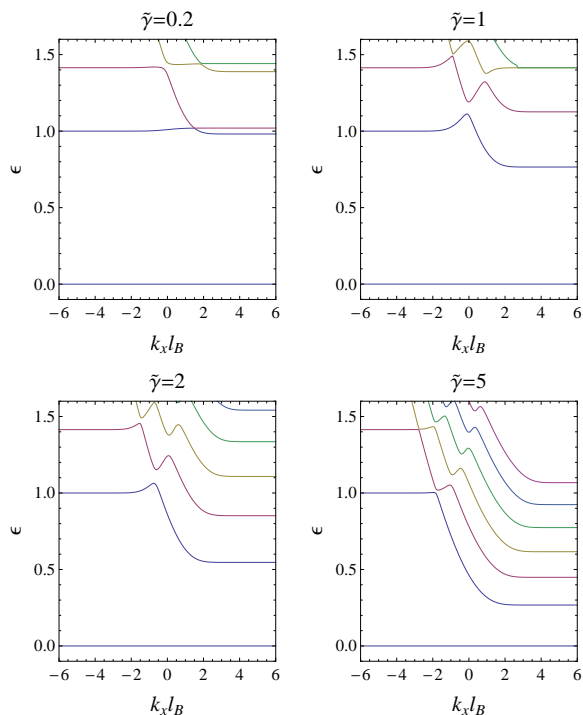


FIG. 8: The dispersion around Dirac cones K of *h.e.b.* type interface in different magnetic field with $\tilde{\gamma} = 0.2, 1, 2, 5$ respectively.

ticrossing in the *h.e.b.* interface. Similar differences between *l.e.b.* and *h.e.b.* interfaces are also discussed for transmission coefficients across the interface^{31,33,34}. For the *h.e.b.* the transmission probability is reduced significantly for incoming electrons with energy $E \sim t_{\perp}$ which can be interpreted in a similar way.

We also see that in presence of magnetic field the dis-

persion of Landau levels continuously goes through the interface in different manners at the two Dirac cones. At Dirac cone $K(K')$, the zero energy Landau levels in the bilayer region split, one branch rises up and becomes the $n = 1$ Landau levels in the monolayer while the other branch remains as zero energy states, and the other higher Landau levels continues from bilayer to monolayer accordingly, i.e. $n = 1|_{\text{bi}} \rightarrow n = 2|_{\text{mono}} \dots$. However, near the other Dirac point $K'(K)$, the zero energy state remains intact, so the other higher Landau levels connect as $n = 1|_{\text{bi}} \rightarrow n = 1|_{\text{mono}} \dots$. We also see an effect of the effective potential barrier imposed by the *h.e.b.* in the dispersive Landau levels near the interface. For a certain range of field strength the dispersion develops a local maximum for *h.e.b.* while the *l.e.b.* only develops a plateau feature.

In summary, the physical properties of hybrid graphene systems are mostly dominated by both that of monolayer and bilayer. The Landau levels remain the same away from the interface. But the existence of dispersive Landau levels near the interface could be related to the unexpected feature other than that of the monolayer and bilayer graphene in the magneto transport experiment²⁸. Further study of the hybrid structures for a more realistic setup, like including edge disorder, gate voltage, etc., are needed to undertake the experimental data.

VI. ACKNOWLEDGEMENT

We wish to thank K. Yang and Y. Barlas for very helpful discussions. This work is supported by Fundamental Research Funds for the Central Universities CDJRC10300007 (Z. X. H) and NSF under Grant No. DMR-1004545 (W.X.D.).

- ¹ K. S. Novoselov, A. K. Geim, S. V. Morozov, D. Jiang, Y. Zhang, S. V. Dubonos, I. V. Grigorieva, and A. A. Firsov, *Science* **306**, 666 (2004).
- ² Y. Zhang, J. P. Small, W. V. Pontius, and P. Kim, *Appl. Phys. Lett.* **86**, 073104 (2005). Y. Zhang, J. P. Small, E.S. Amori, and P. Kim, *Phys. Rev. Lett.* **94**, 176803 (2005).
- ³ J. S. Bunch, Y. Yaish, M. Brink, K. Bolotin, and P. L. McEuen, *Nano Lett.* **5**, 287 (2005).
- ⁴ C. Berger, Z. M. Song, T. B. Li, X. B. Li, A.Y. Ogbazghi, R. Feng, Z.T. Dai, A. N. Marchenkov, E. H. Conrad, P. N. First, and W. A. de Heer, *J. Phys. Chem. B* **108**, 19912 (2004).
- ⁵ K. S. Novoselov, D. Jiang, F. Schedin, T. J. Booth, V. V. Khotkevich, S. V. Morozov, and A. K. Geim, *Proc. Natl. Acad. Sci. USA* **102**, 10451 (2005).
- ⁶ P. R. Wallace, *Phys. Rev.* **71**, 622 (1947).
- ⁷ K. S. Novoselov, A. K. Geim, S. V. Morozov, D. Jiang, M. I. Katsnelson, I. V. Grigorieva, S. V. Dubonos, and A. A. Firsov, *Nature* **438**, 197 (2005); K. S. Novoselov, E. McCann, S. V. Morozov, V. I. Fal'ko, M. I. Katsnelson,

- U. Zeitler, D. Jiang, F. Schedin, and A. K. Geim, *Nature Physics*, **2**, 177 (2006).
- ⁸ Y. Zhang, Y.-W. Tan, H. L. Stormer, and P. Kim, *Nature* **438**, 201 (2005); Y. Zhang, Z. Jiang, J. P. Small, M. S. Purewal, Y.-W. Tan, M. Fazlollahi, J. D. Chudow, J. A. Jaszczak, H. L. Stormer, and P. Kim, *Phys. Rev. Lett.* **96**, 136806 (2006); Z. Jiang, Y. Zhang, H. L. Stormer, and P. Kim, *Phys. Rev. Lett.* **99**, 106802 (2007).
- ⁹ K. S. Novoselov, Z. Jiang, Y. Zhang, S. V. Morozov, H. L. Stormer, U. Zeitler, J. C. Maan, G. S. Boebinger, P. Kim, and A. K. Geim, *Science* **315**, 1379 (2007).
- ¹⁰ D. A. Abanin, K. S. Novoselov, U. Zeitler, P. A. Lee, A. K. Geim, and L. S. Levitov, *Phys. Rev. Lett.* **98**, 196806 (2007).
- ¹¹ A. H. Castro Neto, F. Guinea, N. M. R. Peres, K. S. Novoselov, and A. K. Geim, *Rev. Mod. Phys.* **81**, 109 (2009).
- ¹² S. E. Stein and R. L. Brown, *J. Am. Chem. Soc.* **109**, 3721 (1987).
- ¹³ K. Tanaka, S. Yamashita, H. Yamabe, and T. Yamabe,

- Synth. Met. **17**, 143 (1987).
- ¹⁴ M. Fujita, M. Yoshida, and K. Nakada, Fullerene Sci. Technol. **4**, 565 (1996).
 - ¹⁵ M. Fujita, K. Wakabayashi, K. Nakada, and K. Kusakabe, J. Phys. Soc. Jpn. **65**, 1920 (1996).
 - ¹⁶ K. Nakada, M. Fujita, G. Dresselhaus, and M. Dresselhaus, Phys. Rev. B **54**, 17954 (1996).
 - ¹⁷ H.-X. Zheng, Z. F. Wang, T. Luo, Q. W. Shi, and J. Chen, Phys. Rev. B **75**, 165414 (2007).
 - ¹⁸ L. Brey and H. A. Fertig, Phys. Rev. B **73**, 195408 (2006); **73**, 235411 (2006); H. A. Fertig and L. Brey, Phys. Rev. Lett. **97**, 116805 (2006).
 - ¹⁹ N. M. R. Peres, F. Guinea, and A. H. Castro Neto, Phys. Rev. B **73**, 125411 (2006).
 - ²⁰ M. Kohmoto and Y. Hasegawa, Phys. Rev. B **76**, 205402 (2007).
 - ²¹ S. Ryu and Y. Hatsugai, Phys. Rev. Lett. **89**, 077002 (2002).
 - ²² K. Sasaki, S. Murakami, and R. Saito, Appl. Phys. Lett. **88**, 113110 (2006).
 - ²³ K. Sasaki, K. Sato, R. Saito, J. Jiang, S. Onari, and Y. Tanaka, Phys. Rev. B **75**, 235430 (2007).
 - ²⁴ A. H. Castro Neto, F. Guinea, and N. M. R. Peres, Phys. Rev. B **73**, 205408 (2006).
 - ²⁵ Y. Niimi, T. Matsui, H. Kambara, K. Tagami, M. Tsukada, and H. Fukuyama, Phys. Rev. B **73**, 085421 (2006).
 - ²⁶ Y. Kobayashi, K. Fukui, T. Enoki, K. Kusakabe, and Y. Kaburagi, Phys. Rev. B **71**, 193406 (2005).
 - ²⁷ H. P. Dahal, Z.-X. Hu, N. A. Sinitsyn, K. Yang, and A. V. Balatsky, Phys. Rev. B **81**, 155406 (2010).
 - ²⁸ C. P. Puls, N. E. Staley, and Y. Liu, Phys. Rev. B **79**, 235415 (2009).
 - ²⁹ We have an abstract in APS march meeting which is available online at <http://meetings.aps.org/Meeting/MAR10/Event/119769>.
 - ³⁰ E. V. Castro and N. M. R. Peres and J. M. B. L. Santos, Europhys. Lett. **84**, 17001, (2008).
 - ³¹ J. Nilsson, A. H. Castro Neto, F. Guinea and N. M. R. Peres, Phys. Rev. B, **76**, 165416 (2007).
 - ³² M. Koshino, T. Nakanishi and T. Ando, Phys. Rev. B, **82**, 205436 (2010).
 - ³³ T. Nakanishi, M. Koshino and T. Ando, Phys. Rev. B **82**, 125428 (2010).
 - ³⁴ W. X. Ding, unpublished.